

Iron superhydrides FeH₅ and FeH₆: stability, electronic properties and superconductivity

Alexander G. Kvashnin,^{1,2} Ivan A. Kruglov,^{2,3} Dmitrii V. Semenov,^{1,2} Artem R. Oganov,^{1,2,3,4}

¹ Skolkovo Institute of Science and Technology, Skolkovo Innovation Center 143026, 3 Nobel Street, Moscow, Russian Federation

² Moscow Institute of Physics and Technology, 141700, 9 Institutsky lane, Dolgoprudny, Russian Federation

³ Dukhov Research Institute of Automatics (VNIIA), Moscow 127055, Russian Federation

⁴ International Center for Materials Discovery, Northwestern Polytechnical University, Xi'an, 710072, China

Abstract

Recently a big number of works devoted to search for new hydrides with record high-temperature superconductivity and at the same time the successful synthesis of potential high- T_C superconducting FeH₅ was reported. We present a systematic search for stable compounds in the Fe-H system using variable-composition version of the evolutionary algorithm USPEX. All known (FeH, FeH₃, FeH₅) and several new Fe₃H₅, Fe₃H₁₃ and FeH₆ iron hydrides were found to be stable, resulting in a very complex phase diagram with rich structural relationships between phases. We calculate electronic properties of two potentially high- T_C FeH₅ and FeH₆ phases in the pressure range from 150 to 300 GPa. Indeed, hydrogen-rich FeH₅ and FeH₆ phases were found to be superconducting within Bardeen-Cooper-Schrieffer theory, with T_C values of up to 46 K.

Introduction

Theoretical searches for new iron hydrides attracted attention of the scientific community since 1970s when the phase transitions in the Fe-H system were firstly experimentally investigated under pressure.^{1,2} There are no stable crystalline iron hydrides at ambient conditions, because hydrogen dissolves in iron in a wide range of pressures and temperatures without the formation of individual phases.^{3,4} However such molecules as FeH, FeH₂, Fe₂H₄ and molecular complexes namely FeH₂(H₂)₂, FeH·H₂ and FeH₂(H₂)₃ were identified using infrared spectroscopy at low temperatures in inert gas matrix.⁵⁻⁷ The FeH phase was known as the only one in the Fe-H system for a long time, until the new stable iron hydrides were theoretically predicted in 2012 by Bazhanova et al.⁸ using evolutionary algorithm USPEX with fixed-composition searches (restricted to compositions FeH, FeH₂, FeH₃, FeH₄). New FeH₃ and FeH₄ phases were predicted to be stable at pressure higher than 100 GPa⁸ with evidence for likely stability of FeH₂ at lower pressures. Recently the structural evolution of FeH₄ under pressure was studied as well using fixed-composition search.⁹ Several years later in 2014 Pépin et al.¹⁰ have experimentally synthesized the earlier predicted FeH₃ at 86 GPa. Besides FeH₃ phase another new iron hydride (FeH_{~2}) was experimentally found¹⁰, yet precise positions of hydrogen atoms were not established. Recent experimental investigation by Pépin et al.¹¹ reported about synthesis of FeH₅ at pressures above 130 GPa. Its crystal structure was partially determined using available XRD data, but the exact positions of hydrogen atoms were identified using DFT calculations.³

Recent exceptional interest was attracted to hydrides due to experimental and theoretical findings of high- T_C superconductivity under high pressures.¹²⁻²⁰ Moreover, recent theoretical investigation of new hydrides in the Ge-H system²¹ ($T_C \sim 60$ K), Sn-H¹⁹ ($T_C \sim 100$), MgGeH₆²² ($T_C \sim 132$ K), H-S¹⁴ ($T_C \sim 200$ K) systems and in Th-H²³ and U-H²⁰ systems ($T_C \sim 194$ K) at high pressures as well as landmark achievements in experimental synthesis of H₃S¹⁷ ($T_C \sim 203$ K), PH₃²⁴ ($T_C \sim 100$ K), Si₂H₆²⁵ ($T_C \sim 76$ K) inspire exploration of new hydrides. Fresh theoretical work made by Majumdar et al.²⁶ reported about relatively high possible transition temperature

~ 51 K at 130 GPa in FeH₅. All these findings motivate us to study in details the Fe-H system, in particular, stability and superconducting properties of new phases.

Iron is a distinctive element for superconductivity. It was assumed for a long time that magnetism of iron makes superconductivity impossible. However, in 2001 the superconductivity from non-phonon mechanism of interaction was discovered in nonmagnetic ϵ -Fe with $T_C \sim 2.3$ K at 15 GPa.^{27–29}

Since the unexpected discovery of iron-containing superconducting pnictides in 2008 with potential upper critical magnetic fields of up to 200 T,^{30,31} different mechanisms of superconductivity in such materials in relation with magnetism is still under discussion.³² In this case special interest to FeH₅ is caused by the fact that it is the first synthesized superhydride of iron, where superconductivity could come both from electron-phonon coupling and magneto-elastic coupling in the spin-driven scenario^{33,34} or/and orbital fluctuation pairing^{35,36}.

In the last years many developments have been made in order to extend the scope and predictive power of the USPEX code. One of them was the implementation of variable-composition search³⁷, which allows one to explore the whole compositional space in the studied system in a single calculation. These improvements and previous experimental studies of iron hydrides^{10,11} motivated us to perform the evolutionary variable-composition search for new phases in the Fe-H system. The detailed investigation of stability, structural, electronic and superconducting properties of predicted hydrogen-rich phases was carried out, we estimated the possible contribution of electron-phonon interaction to superconductivity of iron hydrides.

Computational details

We performed variable-composition searches for stable compounds in the Fe-H system at pressure of 0, 50, 100 and 150 GPa using the USPEX^{38,39,37} package. The first generation (120 structures) was created using random symmetric generator, while all subsequent generations (100 structures) contained 20% random structures, and 80% created using heredity, softmutation and transmutation operators. Here, evolutionary searches were combined with structure relaxations using density functional theory (DFT)^{40,41} within the spin-polarized generalized gradient approximation (Perdew-Burke-Ernzerhof, or PBE functional),⁴² and the projector-augmented wave method,^{43,44} as implemented in the VASP package.^{45–47} Plane wave kinetic energy cutoff was set to 600 eV and the Brillouin zone was sampled by Γ -centered k -points meshes with resolution $2\pi \times 0.05 \text{ \AA}^{-1}$.

By definition, a thermodynamically stable phase has the lowest Gibbs free energy (or, at zero Kelvin, lowest enthalpy) among any phase or phase assemblage of the same composition. Thermodynamic convex hull construction compactly presents information about all possible formation and decomposition reactions; phases that are located on the convex hull are the ones stable at given pressure. Stable structures of elemental Fe and H were taken from USPEX calculations and from Refs.^{48–50} and⁵¹, respectively.

Calculations of superconducting T_C were carried out using QUANTUM ESPRESSO package⁵². Phonon frequencies and electron-phonon coupling (EPC) coefficients were computed using density-functional perturbation theory²⁵, employing plane-wave pseudopotential method and PBE exchange-correlation functional⁴². Convergence tests showed that 70 Ry is a suitable kinetic energy cutoff for the plane wave basis set. We used pseudopotentials with PBE exchange-correlation functional. In our calculations of the electron-phonon coupling (EPC) parameter λ , the first Brillouin zone was sampled using $4 \times 4 \times 1$ and $4 \times 4 \times 2$ q -points mesh, and a denser $16 \times 16 \times 4$ and $16 \times 16 \times 8$ k -points mesh for FeH₅ and FeH₆, respectively (with Gaussian smearing and $\sigma = 0.05$ Ry), which approximates the zero-width limits in the calculation of λ .

Electronic band structures of FeH₅ and FeH₆ were calculated using both VASP and QE, and demonstrated good consistency. Comparison of the phonon densities of states calculated using finite displacement method (VASP and PHONOPY^{54,55}) and density-functional perturbation theory (QE) excellent agreement between these methods.

The superconducting transition temperature T_C was estimated by using two equations: "full" – Allen-Dynes and "short" – modified McMillan equation⁵⁶. The "full" Allen-Dynes equation for calculating T_C has the following form⁵⁶:

$$T_C = \omega_{log} \frac{f_1 f_2}{1.2} \exp\left(\frac{-1.04(1 + \lambda)}{\lambda - \mu^* - 0.62\lambda\mu^*}\right), \quad (1)$$

while the modified McMillan equation has the form as:

$$T_C = \frac{\omega_{log}}{1.2} \exp\left(\frac{-1.04(1 + \lambda)}{\lambda - \mu^* - 0.62\lambda\mu^*}\right). \quad (2)$$

The EPC constant λ and logarithmic average frequency ω_{log} were calculated as:

$$\lambda = \int_{\omega_{min}}^{\omega_{max}} \frac{2 \cdot \alpha^2 F(\omega)}{\omega} d\omega \quad (3)$$

and

$$\omega_{log} = \exp\left(\frac{2}{\lambda} \int_{\omega_{min}}^{\omega_{max}} \frac{d\omega}{\omega} \alpha^2 F(\omega) \ln(\omega)\right), \quad (4)$$

and μ^* is the Coulomb pseudopotential, for which we used widely accepted lower and upper bound values of 0.10 and 0.15.

Crystal structures of the predicted phases were generated using VESTA software.⁵⁷

Results and Discussion

In order to predict stable phases in the Fe-H system we performed variable-composition evolutionary searches using the USPEX algorithm^{38,39,37} at pressure range from 0 to 150 GPa. Pressure-composition phase was constructed as shown in Fig. 1. There are no stable hydride phases in the pressure range from 0 to 5 GPa, which is in agreement with experimental observations.^{3,4} Increase of pressure leads to the formation of $Fm\bar{3}m$ -FeH phase which is stable up to 150 GPa. Another experimentally known phase $I4/mmm$ -FeH₂ is magnetic and stable in a relatively narrow pressure range from 45 to 75 GPa, which is in agreement with literature data.¹⁰ New $Pm\bar{3}m$ -Fe₃H₈ becomes stable from 5 until 75 GPa. It is important that $Pm\bar{3}m$ -Fe₃H₈ is structurally similar to $Pm\bar{3}m$ -FeH₃ but with one iron and four hydrogen vacancies in the 4×1×1 supercell of FeH₃ (see Fig. S6 in Supporting Information). At higher pressures it decomposes to the new $P6_3/mmc$ -Fe₃H₅ and $Pm\bar{3}m$ -FeH₃. FeH₃ is stable from 65 to 150 GPa, which agrees with high-pressure experiments where it was synthesized at 86 GPa.¹⁰ $I4/mmm$ -FeH₅ phase recently synthesized¹¹ at pressures above 130 GPa, was found to be thermodynamically stable at pressures from 85 to at least 150 GPa. In the same pressure region the new $I4/mmm$ -Fe₃H₁₃ was theoretically predicted. It is important that newly predicted Fe₃H₅, Fe₃H₈ and Fe₃H₁₃ with compositions close to FeH₂, FeH₃ and FeH₅ display rich polysomatism.⁵⁸

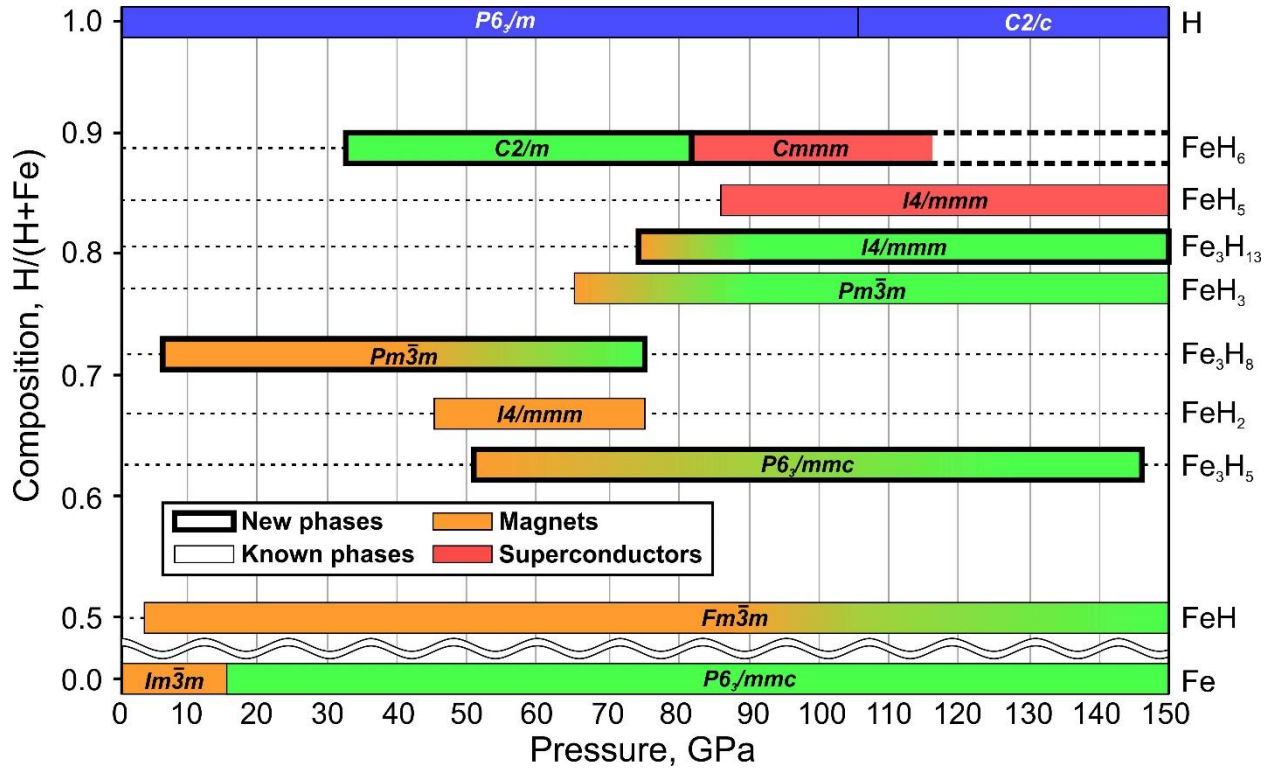


Fig. 1. Pressure-composition phase diagram of the Fe-H system. FeH₅ and FeH₆ are metallic and superconducting. All shown phases, except hydrogen allotropes are metallic.

We also found new hydrogen-rich *C2/m*-FeH₆ phase at pressure higher than 35 GPa to be thermodynamically stable. At ~ 82 GPa *C2/m*-FeH₆ transforms to *Cmmm*-FeH₆ phase (see Fig. 1), which remains thermodynamically stable at pressures up to 115 GPa (see Supporting Information Fig. S1). At higher pressures (up to 150 GPa) *Cmmm*-FeH₆ is only 1.5 meV/atom above decomposition line (see Fig. 2a). Magnetic bcc phase of iron transforms to nonmagnetic hcp ϵ -Fe at 15 GPa (Fig. 1) in agreement with Refs. 27–29. Most of iron hydrides (FeH, Fe₃H₅, Fe₃H₈, FeH₃ and Fe₃H₁₃) are magnetic and become nonmagnetic at high pressures (~ 100 GPa).

Further detailed investigation is devoted to stability, electronic and superconducting properties of Fe-H phases at 150 GPa.

We built the convex hull for the Fe-H system at 150 GPa (see Fig. 2a), which shows that there are 5 stable Fe-H phases namely *Fm3̄m*-FeH, *Pmmm*-Fe₃H₅, *Pm3̄m*-FeH₃, *Immm*-Fe₃H₁₃ and *I4/mmm*-FeH₅. We found a very large number of phases close to convex hull. In the iron-rich part of convex hull (left part of Fig. 2a) the decomposition line has linear character, which corresponds to the formation of solid solutions of hydrogen in iron in a wide range of hydrogen concentrations.^{3,4} Hydrogen-rich region (right part of Fig. 2a) with almost parabolic character of decomposition line and phases at this region display rich polysomatism.⁵⁸ We found *I4/mmm*-FeH₂ to be metastable at 150 GPa by 10 meV/unit. This phase was found in experiments at pressures from 67 GPa up to 86 GPa, but was indicated as FeH₂¹⁰ due to undetermined stoichiometry. Our phase diagram (Fig. 1) explains why FeH₂ was not found at higher pressures.

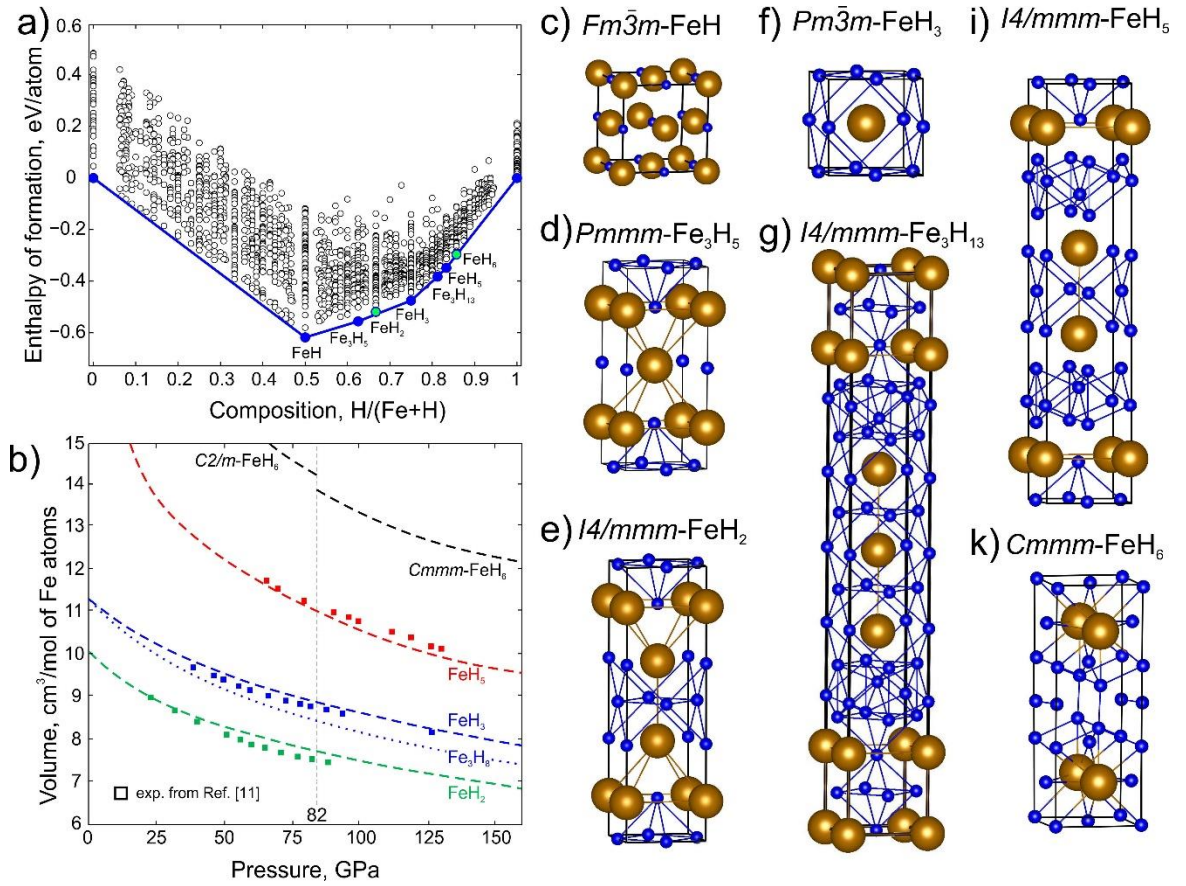


Fig. 2. a) Calculated convex hull of the Fe-H system at 150 GPa. Green points correspond to low-enthalpy metastable FeH_2 and FeH_6 ; b) Equations of state of FeH_2 , Fe_3H_8 , FeH_3 , FeH_5 and FeH_6 phases compared with experimental data from Ref. 11; c-g) Crystal structures of predicted stable Fe-H phases. Iron atoms are shown by large brown balls; hydrogen atoms by small blue balls.

Additionally, we calculated equations of state (EOS) of the predicted FeH_2 , Fe_3H_8 , FeH_3 , FeH_5 and FeH_6 phases and compared them with available experimental data from Refs. ^{10,11} (see Fig. 2b). One can see that theory (dashed lines in Fig. 2b) agrees very well with experimental data (squares in Fig. 2b). EOS of Fe_3H_8 is close to experimental and calculated data for FeH_3 at low pressures (dotted line in Fig. 2b). Comparison of the predicted crystal structures with experiment shows similar positions of iron atoms. Good agreement with all available experimental data lends confidence to our further predictions that the new FeH_6 hydride (see black dashed line in Fig. 2b) should be stable at pressures from 50 GPa (in fact, even lower pressures) to 115 GPa (see Supporting Information).

Crystal structures of FeH , FeH_2 , FeH_3 , FeH_5 and FeH_6 are shown in Fig. 2c-g. FeH phase has the well-known rocksalt-type structure (see Fig. 2c). FeH_2 has orthorhombic structure alternating FeH_3 - and FeH -type layers (see Fig. S7 in Supporting Information). FeH_3 phase (see Fig. 2e) has the smallest unit cell with only 1 iron atom coordinated by 12 hydrogens; together Fe and H atoms occupy sites on the cubic close packing. Predicted Fe_3H_{13} phase has layered structure where each layer is FeH_3 phase with the thickness of 4.7 Å (double unit cell) divided by additional hydrogen layer. FeH_5 phase is similar to Fe_3H_{13} with the only difference in the thickness of FeH_3 -type layers which equals to 2.36 Å (unit cell of FeH_3 phase). Metastable at 150 GPa Cmmm-FeH_6 phase consists of the FeH_3 -type layers, similarly to FeH_5 , but divided by thicker hydrogen layers, than in FeH_5 phase (see Fig. 2b) with H_2 molecules (H-H distance 0.74 Å) between the layers. Such layered structure with alternation of hydrogen and FeH_3 -type layers is similar to Na_3Cl ,⁵⁹ which is made of alternating NaCl and Na_2 layers. It is currently unknown why such alternating-layer polysomatic compounds become stable under pressure.

Our main interest here is in hydrogen-rich FeH_5 and FeH_6 , and their potential superconductivity in view of recent synthesis and investigations of various superconducting hydrides^{12–20,24,25}. It is

important to note that both FeH₅ and FeH₆ remain dynamically stable in the considered pressure region from 150 to 300 GPa, according to phonon calculations (see Supporting Information Fig. S4 and S5).

We have calculated band structures and electronic densities of states of FeH₅ and FeH₆ phases at 150 GPa (see Fig. 3). The atom-projected band structure shows that contribution to the Fermi level mainly comes from iron atoms (red color), while hydrogen bands lie much deeper in conduction and valence bands (blue color). High peaks of the electronic DOS of FeH₅ at -2 eV (see Fig. 3a) can be explained by the presence of flat bands in the direction perpendicular to *c*-axis. Such behavior of the bands indicates the layered structure and weak interaction between layers in FeH₅. All other Fe-H phases are metallic with very low DOS at Fermi level (< 0.15 states/eV/unit).

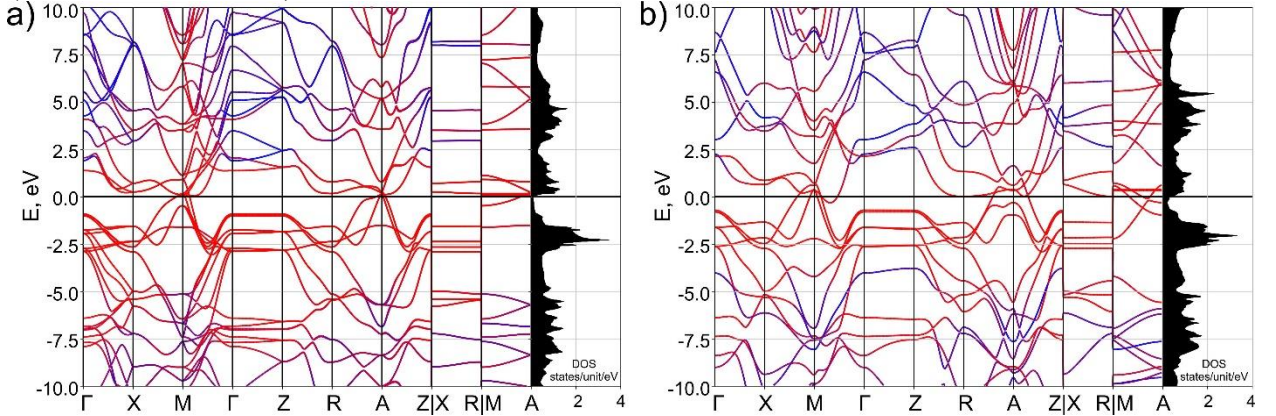


Fig. 3. Electronic band structures and densities of states of a) FeH₅ and b) FeH₆ at 150 GPa. Red color corresponds to the contribution from Fe, while blue color is for hydrogen atoms.

Similarly, the band structure of FeH₆ shows presence of flat bands along the high-symmetry *c*^{*} direction of the reciprocal space (see Fig. 3b). We calculated the electronic DOS for both phases at pressures of 150, 200 and 300 GPa. The values of the densities of states at the Fermi level are shown in Table 1. One can see that as pressure increases the density of states slightly increases as well. (see Table 1).

Both crystal structure and electronic properties of FeH₅ and FeH₆ phase display strong resemblance. We have calculated the electron-phonon coupling (EPC) coefficient λ , logarithmic frequency ω_{\log} and T_C using both Allen-Dynes and McMillan formulas⁵⁶ as a function of pressure (Table 1). One can see that EPC coefficient for FeH₅ phase increases with increasing of pressure due to increasing density of states N_f ($\lambda = N_f \times V_{\text{Coulomb}}$). At the same time T_C decreases with pressure, due to decreasing ω_{\log} . Values of T_C for both phases are reasonably high, ~ 43 -45 K at pressures 150 GPa, which is in a good agreement with data from Ref.²⁶ Below 150 GPa FeH₆ consistently loses its superconducting properties due to changes in the interlayer interactions. Below 100 GPa we have not found superconductivity in FeH₆.

Table 1. Predicted superconducting properties of FeH₅ and FeH₆ phases. T_C values are given for $\mu^* = 0.1$ (0.15).

Phase	<i>P</i> , GPa	λ	N_f , states/unit/eV	ω_{\log} , K	T_C (Allen-Dynes), K	T_C (McMillan), K
FeH ₅	150	0.97	0.145	642.3	45.8 (33.6)	42.6 (32.3)
	200	1.05	0.257	492.7	39.7 (30.6)	36.6 (28.8)
	300	1.26	0.318	339.5	35.7 (28.7)	32.2 (26.5)
FeH ₆	100	0.37	0.731	973.1	3.9 (1.2)	4.0 (1.2)
	150	0.92	0.436	665.6	42.9 (31.3)	40.2 (29.7)
	300	0.94	0.391	549.6	37.3 (27.6)	34.9 (26.1)

Conclusions

Using evolutionary crystal structure prediction algorithm USPEX we have uncovered unexpectedly complex chemistry of the Fe-H system at pressure range from 0 to 150 GPa. We confirmed the atomic structure of the experimentally synthesized FeH₂, FeH₃, FeH₅ and predicted new *Pmmm*-Fe₃H₅, *Immm*-Fe₃H₁₃, *I4/mmm*-FeH₅ and *Cmmm*-FeH₆ phases to be stable at 150 GPa. All predicted new phases belong to the same polysomatic series formed by the FeH- and FeH₃-type blocks. More detailed calculation of *P-V* equation of states allows us to determine the crystal structure of experimentally found FeH₋₂ phase as *I4/mmm*-FeH₂. Determined crystal structure of hydrogen-rich phases allowed us to perform theoretical calculations of electron DOS and superconducting properties within BCS theory. We showed that both FeH₅ and FeH₆ demonstrate electronic behavior corresponding to two-dimensional metals. EPC coefficient and DOS at Fermi level increase with decreasing of ω_{\log} in the pressure range from 150 to 300 GPa, which leads to decrease of T_C . Thus, T_C values for both *I4/mmm*-FeH₅ and *Cmmm*-FeH₆ do not exceed 46 K at 150 GPa.

Acknowledgements

The work was supported by Russian Science Foundation (№ 16-13-10459). Calculations were performed on the Rurik supercomputer at MIPT.

References

- (1) Stevenson, D. J. Hydrogen in the Earth's Core. *Nature* **1977**, 268 (5616), 130–131.
- (2) Wohlfarth, E. P. The Possibility That ϵ -Fe Is a Low Temperature Superconductor. *Phys. Lett. A* **1979**, 75 (1), 141–143.
- (3) Armbruster, M. H. The Solubility of Hydrogen at Low Pressure in Iron, Nickel and Certain Steels at 400 to 600°. *J. Am. Chem. Soc.* **1943**, 65 (6), 1043–1054.
- (4) Da Silva, J. R. G.; Mclellan, R. B. The Solubility of Hydrogen in Super-Pure-Iron Single Crystals. *J. Common Met.* **1976**, 50 (1), 1–5.
- (5) Chertihin, G. V.; Andrews, L. Infrared Spectra of FeH, FeH₂, and FeH₃ in Solid Argon. *J. Phys. Chem.* **1995**, 99 (32), 12131–12134.
- (6) Körsgen, H.; Mürtz, P.; Lipus, K.; Urban, W.; Towle, J. P.; Brown, J. M. The Identification of the FeH₂ Radical in the Gas Phase by Infrared Spectroscopy. *J. Chem. Phys.* **1996**, 104 (12), 4859–4861.
- (7) Wang, X.; Andrews, L. Infrared Spectra and Theoretical Calculations for Fe, Ru, and Os Metal Hydrides and Dihydrogen Complexes. *J. Phys. Chem. A* **2009**, 113 (3), 551–563.
- (8) Bazhanova, Z. G.; Oganov, A. R.; Gianola, O. Fe–C and Fe–H Systems at Pressures of the Earth's Inner Core. *Phys.-Uspekhi* **2012**, 55 (5), 489.
- (9) Li, F.; Wang, D.; Du, H.; Zhou, D.; Ma, Y.; Liu, Y. Structural Evolution of FeH₄ under High Pressure. *RSC Adv.* **2017**, 7 (21), 12570–12575.
- (10) Pépin, C. M.; Dewaele, A.; Geneste, G.; Loubeyre, P.; Mezouar, M. New Iron Hydrides under High Pressure. *Phys. Rev. Lett.* **2014**, 113 (26), 265504.
- (11) Pépin, C. M.; Geneste, G.; Dewaele, A.; Mezouar, M.; Loubeyre, P. Synthesis of FeH₅: A Layered Structure with Atomic Hydrogen Slabs. *Science* **2017**, 357 (6349), 382–385.
- (12) Gao, G.; Oganov, A. R.; Bergara, A.; Martinez-Canales, M.; Cui, T.; Iitaka, T.; Ma, Y.; Zou, G. Superconducting High Pressure Phase of Germane. *Phys. Rev. Lett.* **2008**, 101 (10), 107002.
- (13) Gao, G.; Oganov, A. R.; Li, P.; Li, Z.; Wang, H.; Cui, T.; Ma, Y.; Bergara, A.; Lyakhov, A. O.; Iitaka, T.; et al. High-Pressure Crystal Structures and Superconductivity of Stannane (SnH₄). *Proc. Natl. Acad. Sci.* **2010**, 107 (4), 1317–1320.
- (14) Duan, D.; Liu, Y.; Tian, F.; Li, D.; Huang, X.; Zhao, Z.; Yu, H.; Liu, B.; Tian, W.; Cui, T. Pressure-Induced Metallization of Dense (H₂S)₂H₂ with High- T_C Superconductivity. *Sci. Rep.* **2014**, 4, 6968.

- (15) Hou, P.; Zhao, X.; Tian, F.; Li, D.; Duan, D.; Zhao, Z.; Chu, B.; Liu, B.; Cui, T. High Pressure Structures and Superconductivity of $\text{AlH}_3(\text{H}_2)$ Predicted by First Principles. *RSC Adv.* **2015**, 5 (7), 5096–5101.
- (16) Li, Y.; Hao, J.; Liu, H.; Tse, J. S.; Wang, Y.; Ma, Y. Pressure-Stabilized Superconductive Yttrium Hydrides. *Sci. Rep.* **2015**, 5, 09948.
- (17) Drozdov, A. P.; Erements, M. I.; Troyan, I. A.; Ksenofontov, V.; Shylin, S. I. Conventional Superconductivity at 203 Kelvin at High Pressures in the Sulfur Hydride System. *Nature* **2015**, 525 (7567), 73–76.
- (18) Goncharov, A. F.; Lobanov, S. S.; Kruglov, I.; Zhao, X.-M.; Chen, X.-J.; Oganov, A. R.; Konôpková, Z.; Prakapenka, V. B. Hydrogen Sulfide at High Pressure: Change in Stoichiometry. *Phys. Rev. B* **2016**, 93 (17), 174105.
- (19) Esfahani, M. M. D.; Wang, Z.; Oganov, A. R.; Dong, H.; Zhu, Q.; Wang, S.; Rakitin, M. S.; Zhou, X.-F. Superconductivity of Novel Tin Hydrides (Sn_nH_m) under Pressure. *Sci. Rep.* **2016**, 6, srep22873.
- (20) Kruglov, I. A.; Kvashnin, A. G.; Goncharov, A. F.; Oganov, A. R.; Lobanov, S.; Holtgrewe, N.; Yanilkin, A. V. High-Temperature Superconductivity of Uranium Hydrides at near-Ambient Conditions. *arXiv:1708.05251* **2017**, <https://arxiv.org/abs/1708.05251>.
- (21) Davari Esfahani, M. M.; Oganov, A. R.; Niu, H.; Zhang, J. Superconductivity and Unexpected Chemistry of Germanium Hydrides under Pressure. *Phys. Rev. B* **2017**, 95 (13), 134506.
- (22) Ma, Y.; Duan, D.; Shao, Z.; Yu, H.; Liu, H.; Tian, F.; Huang, X.; Li, D.; Liu, B.; Cui, T. Divergent Synthesis Routes and Superconductivity of Ternary Hydride MgSiH_6 at High Pressure. *Phys. Rev. B* **2017**, 96 (14), 144518.
- (23) Kvashnin, A. G.; Semenok, D. V.; Kruglov, I. A.; Oganov, A. R. High-Temperature Superconductivity in Th-H System at Pressure Conditions. *arXiv:1711.00278* **2017**, <http://arxiv.org/abs/1711.00278>.
- (24) Drozdov, A. P.; Erements, M. I.; Troyan, I. A. Superconductivity above 100 K in PH_3 at High Pressures. *arXiv:1508.06224* **2015**, <http://arxiv.org/abs/1508.06224>.
- (25) Kong, P. P.; Drozdov, A. P.; Eroke, E.; Erements, M. I. Pressure-Induced Superconductivity above 79 K in Si_2H_6 . In *Book of abstracts of AIRAPT 26 joint with ACHPR 8 & CHPC 19*; Bijing, China, 2017; p 347.
- (26) Majumdar, A.; Tse, J. S.; Wu, M.; Yao, Y. Superconductivity in FeH_5 . *Phys. Rev. B* **2017**, 96 (20), 201107.
- (27) Cort, G.; Taylor, R. D.; Willis, J. O. Search for Magnetism in Hcp E-Fe. *J. Appl. Phys.* **1982**, 53 (3), 2064–2065.
- (28) Shimizu, K.; Kimura, T.; Furomoto, S.; Takeda, K.; Kontani, K.; Onuki, Y.; Amaya, K. Superconductivity in the Non-Magnetic State of Iron under Pressure. *Nature* **2001**, 412 (6844), 35085536.
- (29) Yadav, C. S.; Seyfarth, G.; Pedrazzini, P.; Wilhelm, H.; Černý, R.; Jaccard, D. Effect of Pressure Cycling on Iron: Signatures of an Electronic Instability and Unconventional Superconductivity. *Phys. Rev. B* **2013**, 88 (5), 054110.
- (30) Kamihara, Y.; Watanabe, T.; Hirano, M.; Hosono, H. Iron-Based Layered Superconductor $\text{La}[\text{O}_{1-x}\text{F}_x]\text{FeAs}$ ($x = 0.05\text{--}0.12$) with $T_c = 26$ K. *J. Am. Chem. Soc.* **2008**, 130 (11), 3296–3297.
- (31) Zhang, J.; Jiao, L.; Chen, Y.; Yuan, H. Universal Behavior of the Upper Critical Field in Iron-Based Superconductors. *Front. Phys.* **2011**, 6 (4), 463–473.
- (32) Hosono, H.; Kuroki, K. Iron-Based Superconductors: Current Status of Materials and Pairing Mechanism. *Phys. C Supercond. Its Appl.* **2015**, 514 (Supplement C), 399–422.
- (33) Fernandes, R. M.; Chubukov, A. V.; Schmalian, J. What Drives Nematic Order in Iron-Based Superconductors? *Nat. Phys.* **2014**, 10 (2), 2877.
- (34) Eremin, I.; Knolle, J.; Fernandes, R. M.; Schmalian, J.; Chubukov, A. V. Antiferromagnetism in Iron-Based Superconductors: Selection of Magnetic Order and

- Quasiparticle Interference. *J. Phys. Soc. Jpn.* **2014**, 83 (6), 061015.
- (35) Onari, S.; Kontani, H. Self-Consistent Vertex Correction Analysis for Iron-Based Superconductors: Mechanism of Coulomb Interaction-Driven Orbital Fluctuations. *Phys. Rev. Lett.* **2012**, 109 (13), 137001.
 - (36) Yamada, T.; Ishizuka, J.; Ōno, Y. A High-T_c Mechanism of Iron Pnictide Superconductivity Due to Cooperation of Ferro-Orbital and Antiferromagnetic Fluctuations. *J. Phys. Soc. Jpn.* **2014**, 83 (4), 043704.
 - (37) Lyakhov, A. O.; Oganov, A. R.; Stokes, H. T.; Zhu, Q. New Developments in Evolutionary Structure Prediction Algorithm USPEX. *Comput. Phys. Commun.* **2013**, 184, 1172–1182.
 - (38) Oganov, A. R.; Glass, C. W. Crystal Structure Prediction Using Ab Initio Evolutionary Techniques: Principles and Applications. *J Chem Phys* **2006**, 124, 244704.
 - (39) Oganov, A. R.; Lyakhov, A. O.; Valle, M. How Evolutionary Crystal Structure Prediction Works—and Why. *Acc. Chem. Res.* **2011**, 44, 227–237.
 - (40) Hohenberg, P.; Kohn, W. Inhomogeneous Electron Gas. *Phys Rev* **1964**, 136 (3B), B864–B871.
 - (41) Kohn, W.; Sham, L. J. Self-Consistent Equations Including Exchange and Correlation Effects. *Phys Rev* **1965**, 140 (4), A1133–A1138.
 - (42) Perdew, J. P.; Burke, K.; Ernzerhof, M. Generalized Gradient Approximation Made Simple. *Phys. Rev. Lett.* **1996**, 77 (18), 3865–3868.
 - (43) Blöchl, P. E. Projector Augmented-Wave Method. *Phys. Rev. B* **1994**, 50 (24), 17953–17979.
 - (44) Kresse, G.; Joubert, D. From Ultrasoft Pseudopotentials to the Projector Augmented-Wave Method. *Phys. Rev. B* **1999**, 59 (3), 1758–1775.
 - (45) Kresse, G.; Furthmüller, J. Efficient Iterative Schemes for Ab Initio Total-Energy Calculations Using a Plane-Wave Basis Set. *Phys. Rev. B* **1996**, 54, 11169–11186.
 - (46) Kresse, G.; Hafner, J. Ab Initio Molecular Dynamics for Liquid Metals. *Phys. Rev. B* **1993**, 47, 558–561.
 - (47) Kresse, G.; Hafner, J. Ab Initio Molecular-Dynamics Simulation of the Liquid-Metal Amorphous-Semiconductor Transition in Germanium. *Phys. Rev. B* **1994**, 49, 14251–14269.
 - (48) Saxena, S. K.; Dubrovinsky, L. S.; Häggkvist, P.; Cerenius, Y.; Shen, G.; Mao, H. K. Synchrotron X-Ray Study of Iron at High Pressure and Temperature. *Science* **1995**, 269 (5231), 1703–1704.
 - (49) Belonoshko, A. B.; Ahuja, R.; Johansson, B. Stability of the Body-Centred-Cubic Phase of Iron in the Earth's Inner Core. *Nature* **2003**, 424 (6952), 1032–1034.
 - (50) Tateno, S.; Hirose, K.; Ohishi, Y.; Tatsumi, Y. The Structure of Iron in Earth's Inner Core. *Science* **2010**, 330 (6002), 359–361.
 - (51) Pickard, C. J.; Needs, R. J. Structure of Phase III of Solid Hydrogen. *Nat. Phys.* **2007**, 3 (7), 473–476.
 - (52) Giannozzi, P.; Baroni, S.; Bonini, N.; Calandra, M.; Car, R.; Cavazzoni, C.; Ceresoli, D.; Chiarotti, G. L.; Cococcioni, M.; Dabo, I.; et al. QUANTUM ESPRESSO: A Modular and Open-Source Software Project for Quantum Simulations of Materials. *J. Phys. Condens. Matter* **2009**, 21, 395502.
 - (53) Baroni, S.; de Gironcoli, S.; Dal Corso, A.; Giannozzi, P. Phonons and Related Crystal Properties from Density-Functional Perturbation Theory. *Rev. Mod. Phys.* **2001**, 73 (2), 515–562.
 - (54) Togo, A.; Tanaka, I. First Principles Phonon Calculations in Materials Science. *Scr. Mater.* **2015**, 108, 1–5.
 - (55) Togo, A.; Oba, F.; Tanaka, I. First-Principles Calculations of the Ferroelastic Transition between Rutile-Type and CaCl₂-Type SiO₂ at High Pressures. *Phys. Rev. B* **2008**, 78, 134106.
 - (56) Allen, P. B.; Dynes, R. C. Transition Temperature of Strong-Coupled Superconductors Reanalyzed. *Phys. Rev. B* **1975**, 12 (3), 905–922.
 - (57) Momma, K.; Izumi, F. VESTA 3 for Three-Dimensional Visualization of Crystal,

- Volumetric and Morphology Data. *J. Appl. Crystallogr.* **2011**, *44*, 1272–1276.
- (58) Veblen, D. R. Polysomatism and Polysomatic Series: A Review and Applications. *Am. Mineralogist* **1991**, *76*, 801–826.
- (59) Zhang, W.; Oganov, A. R.; Goncharov, A. F.; Zhu, Q.; Boulfelfel, S. E.; Lyakhov, A. O.; Somayazulu, M.; Prakapenka, V. B. Unexpected Stable Stoichiometries of Sodium Chlorides. *Science* **2013**, *342* (6165 DOI-10.1126/science.1244989), 1502–1505.

Supporting information

Iron superhydrides FeH₅ and FeH₆: stability, electronic properties and superconductivity

Alexander G. Kvashnin,^{1,2} Ivan A. Kruglov,^{2,3} Dmitrii V. Semenov,^{1,2} Artem R. Oganov,^{1,2,3,4}

¹ Skolkovo Institute of Science and Technology, Skolkovo Innovation Center 143026, 3 Nobel Street, Moscow, Russian Federation

² Moscow Institute of Physics and Technology, 141700, 9 Institutsky lane, Dolgoprudny, Russian Federation

³ Dukhov Research Institute of Automatics (VNIIA), Moscow 127055, Russian Federation

⁴ International Center for Materials Discovery, Northwestern Polytechnical University, Xi'an, 710072, China

Equations for calculation T _C	12
Stability ranges of new iron polyhydrides	12
Crystal structures of FeH, FeH ₂ , FeH ₃ and Fe ₃ H ₈ phases.....	14
Electronic properties of Fe-H phases	15
Eliashberg spectral functions for FeH ₅ , FeH ₆ phases at different pressures.....	15
References.....	17

Equations for calculation T_C

The “full” Allen-Dynes equation for calculating T_C has the following form ¹:

$$T_C = \omega_{log} \frac{f_1 f_2}{1.2} \exp\left(\frac{-1.04(1 + \lambda)}{\lambda - \mu^* - 0.62\lambda\mu^*}\right), \quad (S5)$$

while the modified McMillan equation has the form as:

$$T_C = \frac{\omega_{log}}{1.2} \exp\left(\frac{-1.04(1 + \lambda)}{\lambda - \mu^* - 0.62\lambda\mu^*}\right), \quad (S6)$$

where

$$f_1 = \left(1 + \left(\frac{\lambda}{\Lambda_1}\right)^{\frac{3}{2}}\right)^{\frac{1}{3}}, \quad f_2 = 1 + \frac{\lambda^2}{\lambda^2 + \Lambda_2^2} \cdot \left(\frac{\omega_2}{\omega_{log}} - 1\right) \quad (S7)$$

and

$$\Lambda_1 = 2.46(1 + 3.8\mu^*), \quad \Lambda_2 = 1.82(1 + 6.3\mu^*),$$

$$\omega_2 = \sqrt{\frac{1}{\lambda} \int_{\omega_{min}}^{\omega_{max}} \left[\frac{2 \cdot a^2 F(\omega)}{\omega} \right] \omega^2 d\omega} \quad (S8)$$

f_1 , f_2 , Λ_1 , Λ_2 are functions and correlation factors, used in Allen-Dynes paper for calculating the critical temperature in the case of the inapplicability of the McMillan approximation for large EPC parameters $\lambda > 2$, ω_2 is square root of the mean squared frequency. Minimal ($\omega_{min} > 0$) and maximal (ω_{max}) frequencies were determined as the extreme zero values of the Eliashberg function, where $a^2 F(\omega) < 10^{-6}$.

Stability ranges of new iron polyhydrides

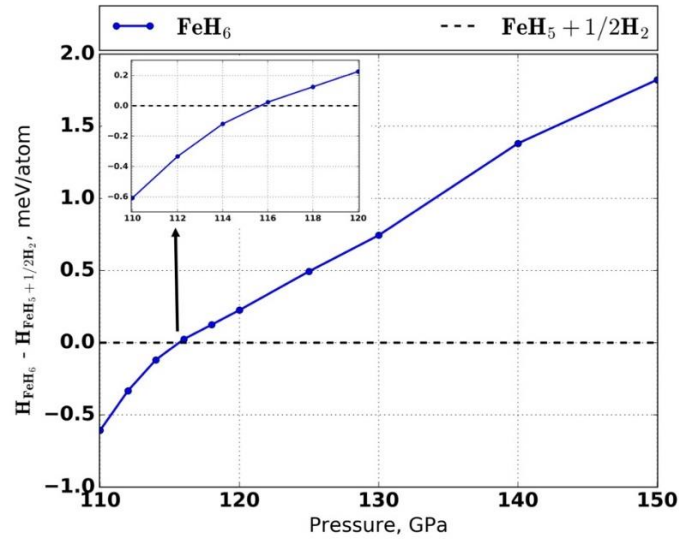


Fig. S1. Decomposition enthalpy curve of FeH_6 into FeH_5 and H_2 .

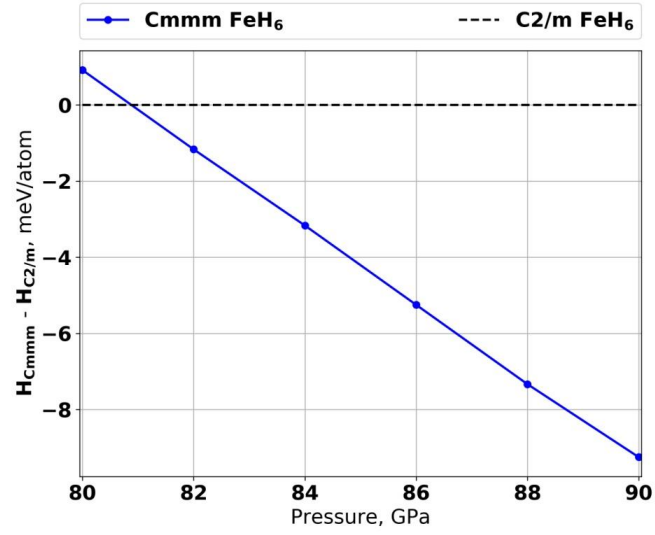


Fig. S2. Enthalpy difference between *Cmmm* and *C2/m*-FeH₆ phases.

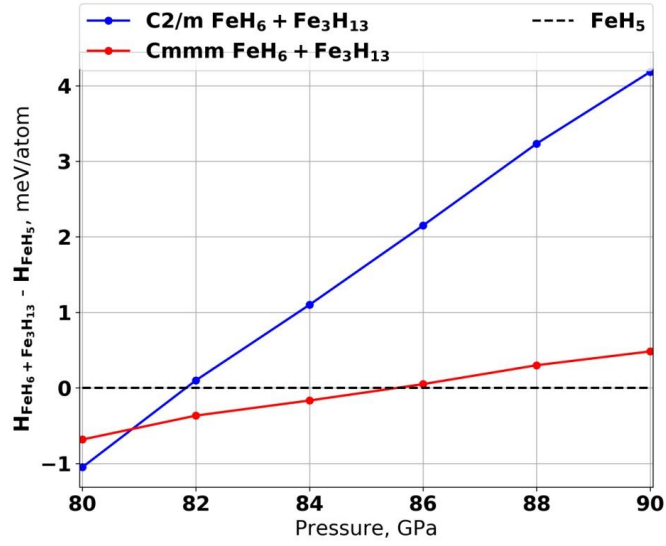


Fig. S3. Enthalpy of formation of FeH₅ formation from FeH₆ and Fe₃H₁₃

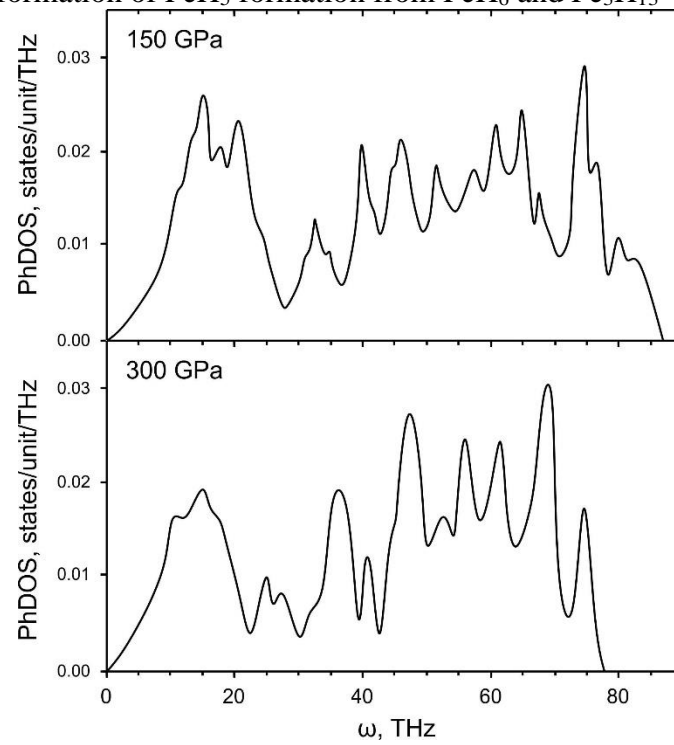


Fig. S4. Phonon DOS of FeH₅ at 150 and 300 GPa.

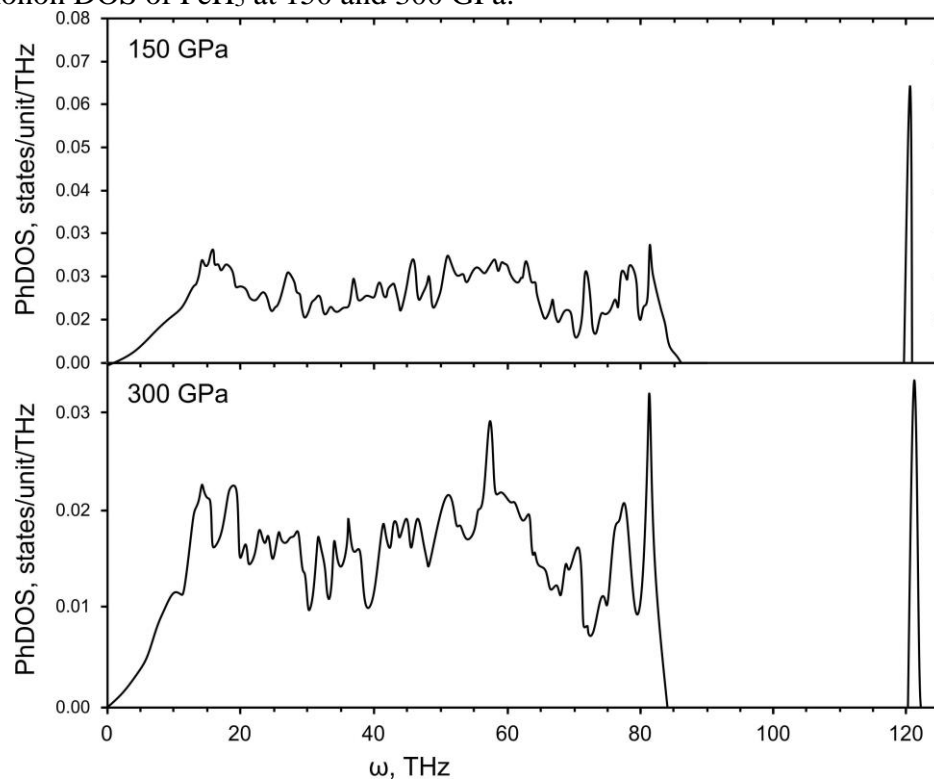


Fig. S5. Phonon DOS of FeH₆ at 150 and 300 GPa.

Crystal structures of FeH, FeH₂, FeH₃ and Fe₃H₈ phases

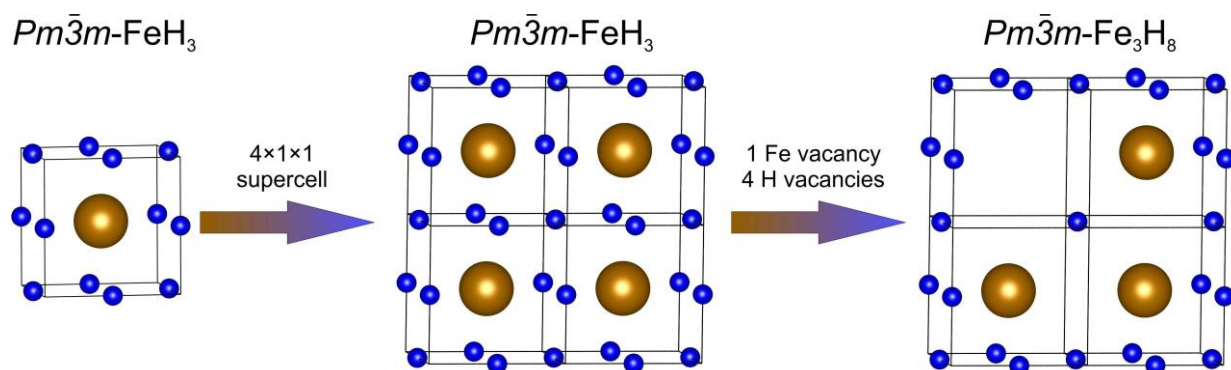


Fig. S6. Similarity between crystal structure of FeH₃ and Fe₃H₈. One iron and four hydrogen vacancies transform 4×1×1 supercell of FeH₃ to Fe₃H₈.

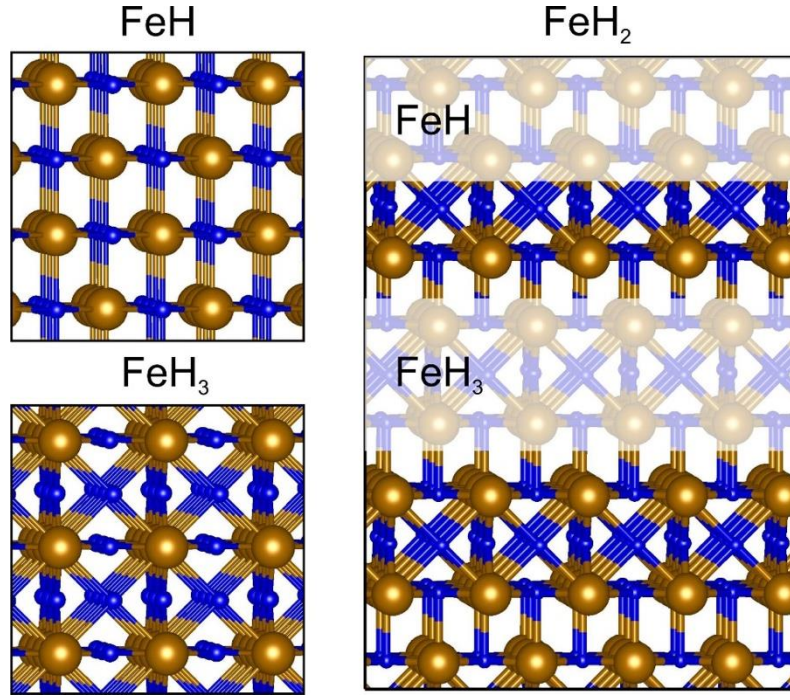


Fig. S7. Crystal structures of Fe-H phase showing the alternation of FeH- and FeH₃-type layers along *c*-axis in FeH₂ phase.

Electronic properties of Fe-H phases

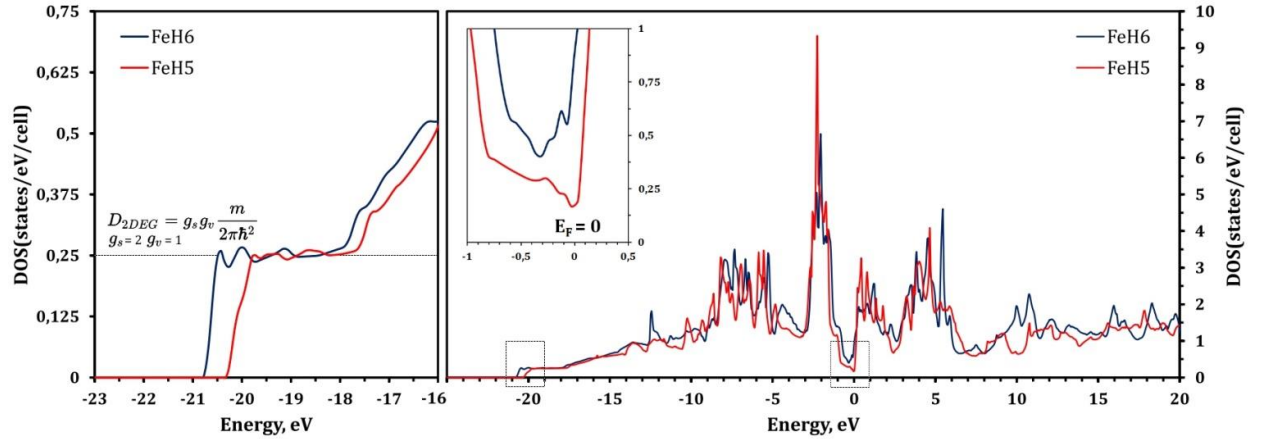


Fig. S8. Electronic density of states for *Fm* $\bar{3}$ *m*-FeH₅ and *Cmmm*-FeH₆ phases at 150 GPa.

As can be seen from the Fig. S6 the DOS(*E*) functions can be considered as combinations of 2 contributions: interlayer electronic density of states (3D) and intralayer density of states (2D) localized between the iron atoms in the layers. The latter contribution numerically equals to 0.25 states/eV/cell (the cell parameters of 2D FeH₅ sublattice at 150 GPa are *a* = *b* = 2.39 Å) and clearly manifests itself near Fermi level (see inset of right panel of Fig. S8) and in the region from -17.5 to -20 eV, where the 3D contribution is almost zero (inset of left panel of Fig. S8). Two-dimensional density of states does not depend on energy and identifying by the characteristic step (see inset of left panel of Fig. S8). Moreover, the intralayer conductivity causes the metallic properties of FeH₅, FeH₆ at 150 GPa.

Eliashberg spectral functions for FeH₅, FeH₆ phases at different pressures

In these all cases the stretch contribution is weak (from 120 to 140 THz) and has not shown on the diagram for clarity

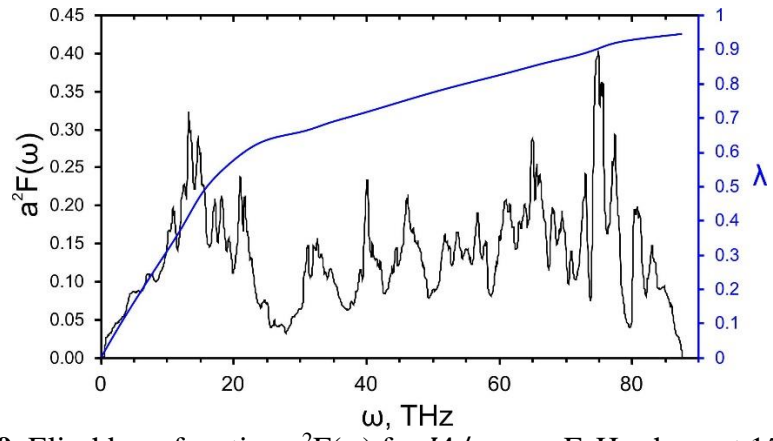


Fig. S9. Eliashberg function $a^2F(\omega)$ for $I4/mmm$ -FeH₅ phase at 150 GPa

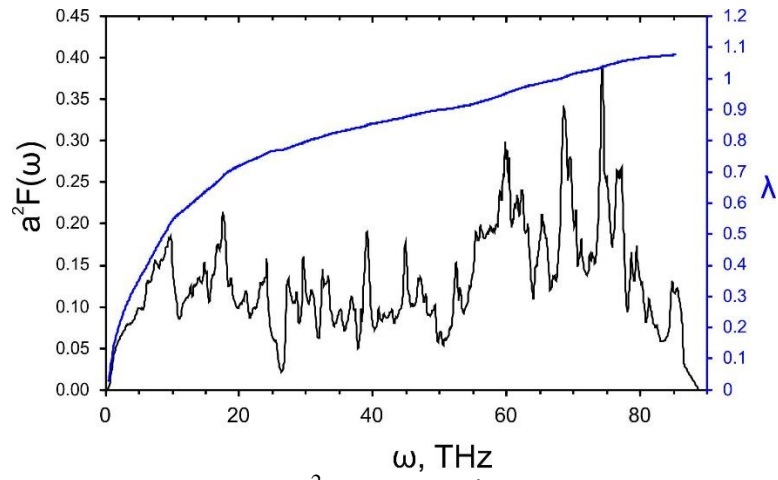


Fig. S10. Eliashberg function $a^2F(\omega)$ for $I4/mmm$ -FeH₅ phase at 200 GPa

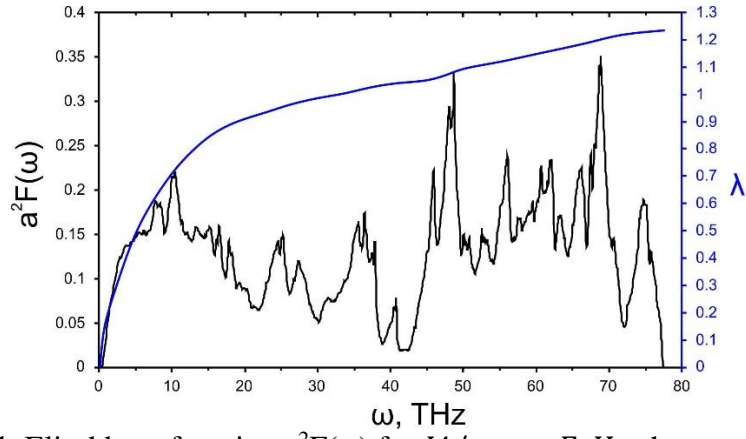


Fig. S11. Eliashberg function $a^2F(\omega)$ for $I4/mmm$ -FeH₅ phase at 300 GPa

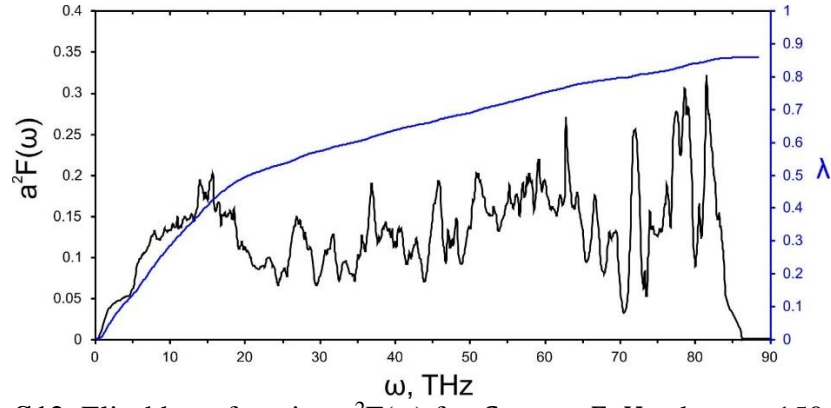


Fig. S12. Eliashberg function $a^2F(\omega)$ for $Cmmm$ -FeH₆ phase at 150 GPa

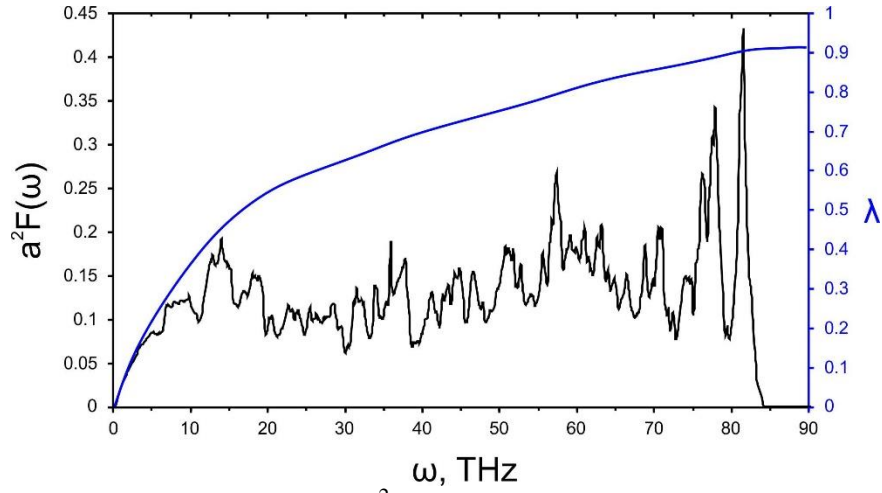


Fig. S13. Eliashberg function $a^2F(\omega)$ for $Cmmm$ -FeH₆ phase at 300 GPa

References

- (1) Allen, P. B.; Dynes, R. C. Transition Temperature of Strong-Coupled Superconductors Reanalyzed. *Phys. Rev. B* **1975**, *12*, 905–922.